Materials Advances

ROYAL SOCIETY OF CHEMISTRY

PAPER

View Article Online
View Journal | View Issue

Cite this: *Mater. Adv.*, 2026, 7, 1531

Crystal engineering focusing on intermolecular CH–π interactions in the 1,4-distyrylbenzene backbone for organic crystal laser media

Takumi Matsuo, *[ab] Daisuke Furusho,[c] Shinsuke Inagi[c] and Shotaro Hayashi *[ab]

Received 22nd October 2025,
Accepted 1st November 2025

DOI: 10.1039/d5ma01220a

rsc.li/materials-advances

Single-crystals composed of organic π-conjugated molecules with high solid-state luminescence are promising candidates for laser media. Among them, *trans*,*trans*-1,4-distyrylbenzene (**DSB**) derivatives are particularly attractive due to their high photoluminescence and are frequently employed in systems of laser media and amplified spontaneous emissions (ASE). Although numerous **DSB** derivatives have been designed for single-crystal laser applications, achieving high solid-state luminescence remains challenging because of the difficulty in predicting and controlling aggregation motifs. We report herein a chemical structure design strategy based on fluorination of **DSB**s to achieve ASE. The fluorination at the central phenylene of **DSB** effectively inhibited intermolecular CH–π interactions. In contrast, the fluorination at the α- or β-position in the vinylene unit did not suppress such interactions, resulting in CH–π interaction-driven herringbone packing. The fluorinated **DSB**s exhibiting herringbone packing in the crystal-state demonstrate ASE due to the high luminescence performance based on the small intermolecular overlapping of their π-orbitals.

Introduction

Organic π-conjugated molecules have been paid significant attention in recent years due to their facile HOMO–LUMO level tunability and the ability to modulate their optoelectronic properties. Among them, organic single-crystals (OSCs) exhibit superior performance in luminescence and charge carrier transport owing to their highly ordered and large-scale molecular alignment. Based on this alignment, OSCs with high luminescence efficiency are promising materials for the development of photonic integrated circuits (PICs), incorporating the functionalities such as lasers or amplified spontaneous emitters (ASEs),[1–12] optical cavities,[13,14] and optical waveguides.[15–26]

To realize these photonic functionalities, π-conjugated molecules with high solid-state luminescence performance have been extensively developed. In particular, the molecules exhibiting aggregation-induced emission (AIE) or aggregation-induced enhanced emission (AIEE) are considered promising candidates for use in OSC-based photonic applications. A wide variety of AIE- and AIEE-active molecules have been reported to date. Among them, π-conjugated molecular structures consisting of alternating phenylene and vinylene units such as *trans*-*trans*-1,4-distyrylbenzenes (**DSB**s) have been widely utilized as representative frameworks.[27–30] **DSB** derivatives with high photoluminescence (PL) performance have been actively studied and developed for OSC laser applications.[2]

Among the various applications of OSC photonics, the development of OSC lasers remains particularly challenging due to the stringent requirements for high solid-state luminescence efficiency and stability. Despite significant efforts, a rational molecular design strategy for OSC laser materials has not yet been established, primarily due to the difficulty in controlling the aggregation motif. In recent years, the relationship between aggregation motifs and laser performance has been increasingly studied.[2] However, effective molecular design strategies to translate into laser-active materials remain limited. Although the electronic energy levels of π-conjugated molecules can be readily modulated through synthetic substitutions, the resulting molecular conformation and packing motifs in the crystal can be unpredictably altered due to complex intra- or intermolecular interactions or unexpected steric hindrance introduced substituents.

Among various types of substituents, halogen atoms are smaller than other commonly used substituents in π-conjugated molecules for optoelectronic applications such as methyl, methoxy, or cyano-groups. This compact property of halogen atoms helps minimize the risk of unexpected steric

[a] *School of Engineering Science, Kochi University of Technology, Kami, Kochi 782-8502, Japan. E-mail: matsuo.takumi@kochi-tech.ac.jp*
[b] *FOREST Center, Research Institute, Kochi University of Technology, Kami, Kochi 782-8502, Japan*
[c] *Department of Chemical Science and Engineering, School of Materials and Chemical Technology, Institute of Science Tokyo, 4259 Nagatsuta-cho, Yokohama 226-8501, Japan*

hindrance in the aggregation motif. Among them, the fluorine atom is the lightest halogen atom, which reduces the potentiality of the heavy atom effect and thus helps preserve luminescence efficiency. In recent years, fluorination of π-conjugated molecules has been employed to enhance their optoelectronic properties. Fluorinated π-conjugated molecules have demonstrated high photoluminescence efficiency and efficient charge carrier transportation.[31–35] Despite these advantages, laser media applications of fluorinated π-conjugated molecules remain largely unexplored.

To elucidate the relationship between the chemical structure, crystal structure, and luminescence performance, it is ideal to use a simplified molecular framework. Herein, we propose a rational crystal engineering strategy based on the fluorination on one of the most commonly used AIEE backbones; **DSB**s, for the discovery of efficient OSC laser media. We found that the position of the fluorination has a significant impact on the aggregation motif, as well as on the luminescence and the ASE performance. **DSB** consists of three phenylene units and two vinylene linkers. Fluorination on the central phenylene unit strongly suppresses intermolecular CH–π interactions, resulting in a π-stacked aggregation motif. In contrast, fluorination at the vinylene units preserves intermolecular CH–π interactions, leading to the herringbone packing structures. The design strategy of this study is illustrated in Fig. 1.

Results and discussion

Molecules **1**, **2**, and **3** were synthesized following the literature.[30] Crystals of **1** and **2** were obtained *via* a solution process. To obtain the crystals, dichloromethane solution of **1** or **2** was evaporated in a fume hood. Fig. 2 shows the PL and its excitation (PLE) spectra measured for each crystal (PL: red, PLE: blue). Fig. 2a–c show the spectra measured for crystals of **1**, **2**, and **3**, respectively. Each crystal exhibited a blue or greenish blue luminescent colour. Each crystal exhibited spectra with vibronic transitions, which indicated the highly luminescent properties.

Fig. 3 shows the crystal structures of the compounds **1**, **2**, and **3**, respectively. Fig. 3a–c show the crystal structure of compound **1**. In Fig. 3a, the packing between two neighbouring molecules suggests the presence of intermolecular CH–π interactions. Fig. 3b shows molecular packing from a different projection, revealing a herringbone arrangement. Fig. 3c shows the crystal structure projected along the *ac*-plane, highlighting the uniaxial orientation of the molecular long-axis, which was suggested to be the ideal orientation for laser media because of the efficient stimulated emissions. Similarly, **2** exhibited CH–π interactions, herringbone packing, and uniaxial molecular arrangement (Fig. 3d–f). In contrast, compound **3** exhibited intermolecular π–π stacking, as shown in Fig. 3g and h, attributed to the fluorination on the central phenylene unit of the **DSB** backbone. The images in Fig. 3 show the plausible crystal morphology. In the case of π-conjugated molecules showing herringbone packing, crystals grow along the direction of CH–π interactions. Owing to the presence of two such interaction directions, the crystals form a platelet morphology. In addition, the π-conjugated molecules with slipped face-to-face stacking crystallize along the directions of intermolecular π–π stacking. To further investigate the relationship between the fluorination position and the aggregation motif, we analysed the crystal structures of four **DSB** molecules substituted with two fluorine atoms (Fig. S9), namely **4**, **5**, **6**, and **7**, respectively (CCDC deposition numbers: 2475422 for **4**, 2475424 for **5**, 2475425 for **6**, and 2475426 for **7**). These synthetic processes are shown in Scheme S1. The corresponding ^{1}H and ^{13}C NMR spectra are shown in Fig. S1–S8. Compound **4**, fluorinated at the central phenylene, exhibited a π-stacked aggregation motif. In contrast, compounds **5**, **6**, and **7**, fluorinated at the terminal phenylene ring, exhibited CH–π aggregation motifs. These results strongly support our proposed strategy: fluorination at the central phenylene unit induces π-stacked packing, while fluorination at the other position enables controlled modulation of the aggregation. PL and PLE spectra are shown in Fig. S10. Each crystal exhibited vibronically structured spectra, indicative of their highly luminescent properties. In the case of solid-state organic π-conjugated molecules with high luminescence efficiency, vibronic transitions are commonly observed. In contrast, broad PL spectra appear for the case of solids with an excimer emission motif.

Based on the stacking manners of the molecules in crystals, we measured the ASE spectra to evaluate their potential as crystal laser media. Fig. 4a shows the PL spectra of compound **1** at varying excitation fluences; I_{ex} (mJ cm^{-2}). At I_{ex} below 4.5 mJ cm^{-2}, broad PL spectra with vibronic progressions appeared. In contrast, at I_{ex} above 4.5 mJ cm^{-2}, sharp and intense PL spectra appeared at 444 nm. Fig. 4b shows the dependence of the integrated PL intensity on I_{ex}. A superlinear increase in intensity was observed with increasing I_{ex} indicating a threshold at 4.5 mJ cm^{-2}. Thus, the crystal of compound **1** exhibited ASE. Fig. 4c presents PL spectra of compound **2** under varying excitation fluences. At I_{ex} below 3.1 mJ cm^{-2}, broad PL spectra with vibronic progressions were observed. Above 3.1 mJ cm^{-2}, a sharp and intense emission peak appeared at 465 nm. Fig. 4d shows the integrated PL intensity as a function of I_{ex}, displaying a superlinear increase with a threshold at

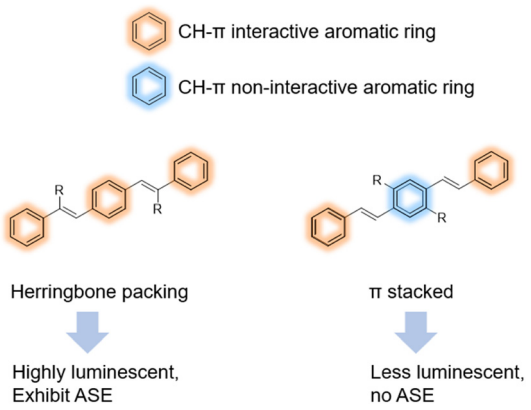

Fig. 1 Schematic depiction of the design strategy used in this work.

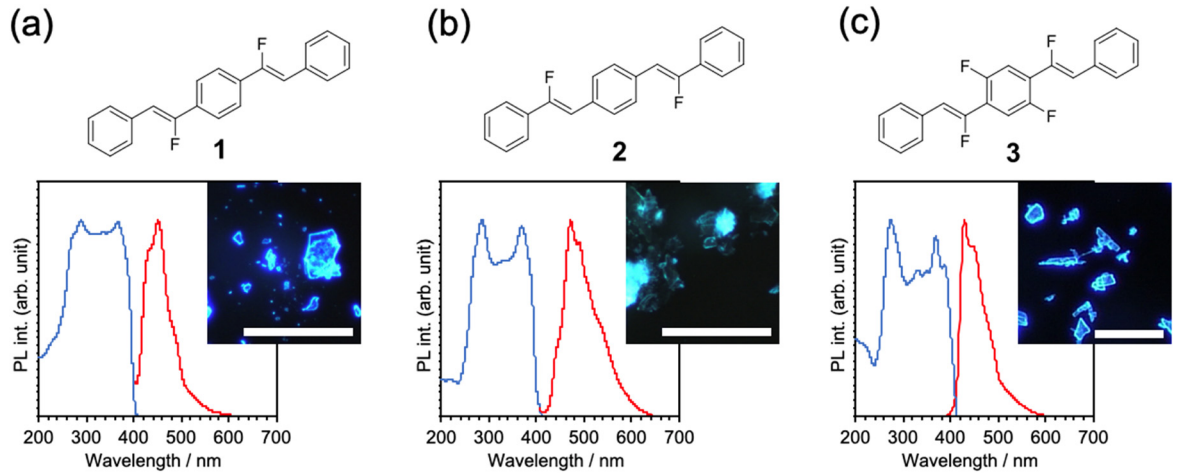

Fig. 2 PL and PLE spectra measured for crystals of (a) **1**, (b) **2**, and (c) **3**, respectively (PL: red, PLE: blue). Each graph contains their chemical structure (scale bar: 500 μm for images of crystals **1** and **2**, 200 μm for crystal **3**).

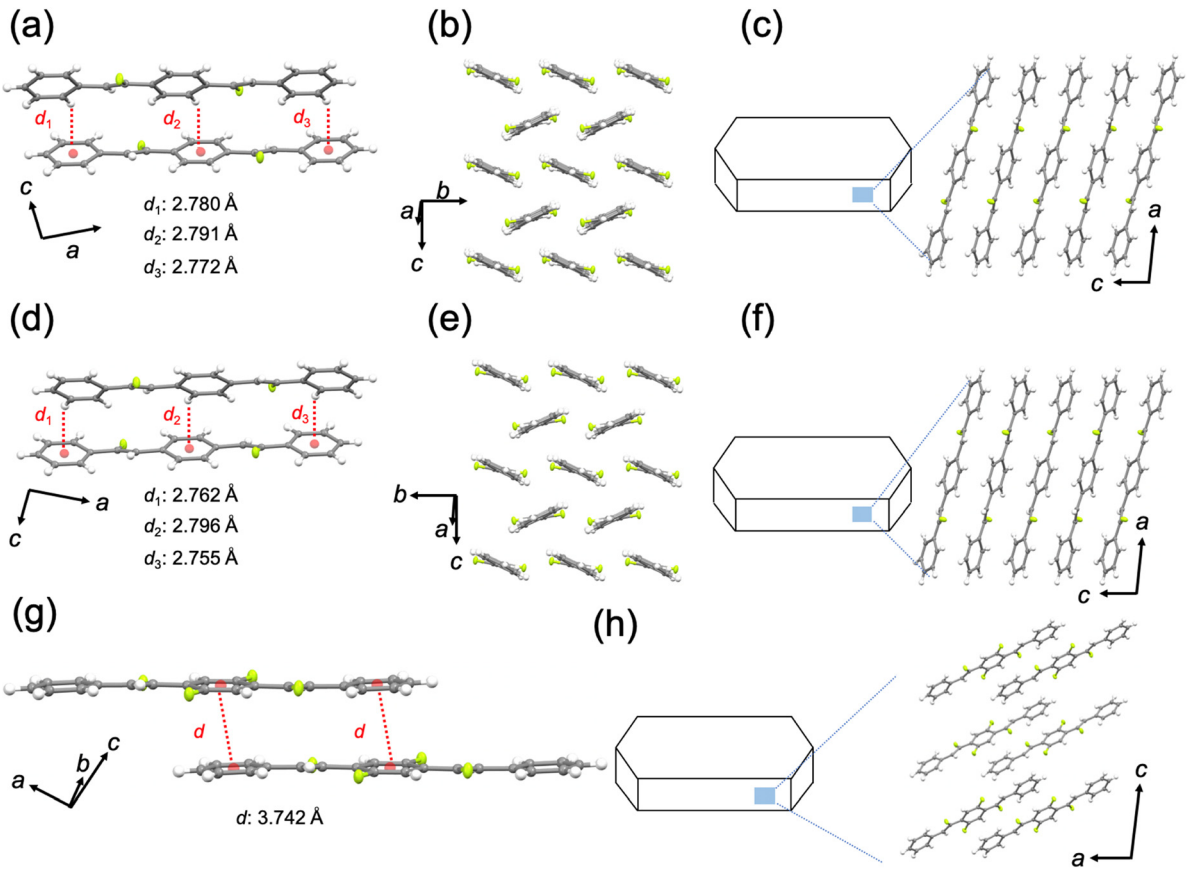

Fig. 3 Crystal structures of (a)–(c) **1**, (d)–(f) **2**, and (g) and (h) **3**, respectively.

3.12 mJ cm^{-2}. These results indicate that the crystal of compound **2** also exhibited ASE. In contrast, the crystal of compound **3** did not show such a gain-narrowing behaviour, likely due to reduced luminescence performance based on the π–π stacking.

To further investigate the origin of the ASE performance, PL lifetime measurement was performed. The average PL lifetime (τ_F) values were estimated to be 0.96 ns, 0.80 ns, 1.39 ns for crystals of compounds **1**, **2**, and **3**, respectively (Fig. S11). The PL quantum efficiency (Φ_{PL}) values in the solid-state were reported to be 0.51, 0.48, 0.25 for crystals **1**, **2**, and **3**, respectively.[30] Based on these values, the radiative rate constants (k_r) were calculated using the equation $k_r = \Phi_{PL}/\tau_F$,

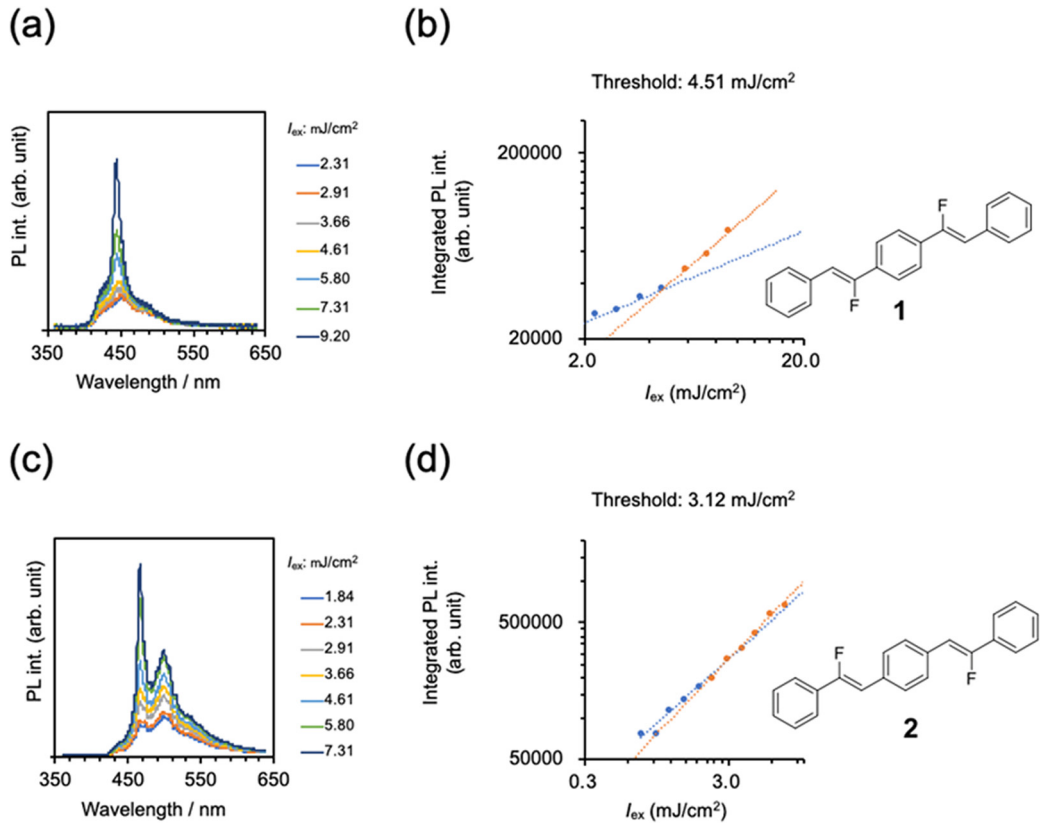

Fig. 4 (a) PL spectra taken for a crystal of **1** measured at each I_{ex} and (b) I_{ex} dependence on the integrated PL intensity. (c) PL spectra taken for a crystal of **2** measured at each I_{ex} and (d) I_{ex} dependence on the integrated PL intensity.

yielding 0.53 ns^{-1}, 0.60 ns^{-1}, and 0.18 ns^{-1} for crystals **1**, **2**, and **3**, respectively. The significantly lower k_r value of crystal **3** compared to those of crystals **1** and **2** is attributed to excimer-like luminescence, originating from the π-stacked aggregation motif. According to the literature, the k_r value of **DSB** was reported to be 0.30 ns^{-1}.[27] These results suggest that the fluorination at the vinylene unit of **DSB** enhances the luminescence performance. The results of optical characterization are summarized in Table 1. While multiple parameters influence the ASE behaviour, the key parameter is k_r values.[4] The enhanced k_r values observed for crystals **1** and **2**, compared to crystal **3** and unsubstituted **DSB** suggest a segregated aggregation motif. In the crystal structure of **DSB**, intermolecular short contacts are observed between a pair of the closest molecules. In contrast, such short contacts are absent in the crystal structures of **1** and **2**, implying that π-orbital overlap is more effectively suppressed in these compounds. This suppression may result from the electrostatic repulsion of the introduced fluorine atoms. Time-dependent density functional theory (TD-DFT) calculations for crystal structures of **1**, **2**, and **3** are shown in Fig. S12–S14. Each result indicates the well-overlapped HOMO–LUMO orbitals.

Table 1 Optical properties of **DSB** crystals

	Φ_{PL}	τ_F/ns	k_r/ns^{-1}	k_{nr}/ns^{-1}
DSB	0.53	1.76	0.30	0.27
1	0.51	0.96	0.53	0.51
2	0.48	0.80	0.60	0.65
3	0.25	1.39	0.18	0.54

Experimental

Chemicals

All solvents were used as received.

Synthesis

1, **2**, and **3** were synthesized following the literature.[30]

Crystal growth

Crystal growth of **1**: 2.1 mg of molecular powder was dissolved in 3.1 mL of dichloromethane. Then, the solvent was evaporated in a fume hood at room temperature.

Crystal growth of **2**: 3.2 mg of molecular powder was dissolved in 3.2 mL of dichloromethane. Then, the solvent was evaporated in a fume hood at room temperature.

Crystal of **3** was prepared without intended growth after the synthesis.

Measurements

Unless otherwise noted, all the experiments were conducted at room temperature (25 ± 3 °C). Liquid-state ^1H (400 MHz) and

^{13}C (100 MHz) nuclear magnetic resonance (NMR) spectra were recorded on a JEOL ECZ400S. Chemical shifts (δ) were expressed relative to the resonances of the residual non-deuterated solvents for ^{1}H [$CDCl_3$: ^{1}H(δ) = 7.26 ppm] or ^{1}H [DMSO_d_6: ^{1}H(δ) = 2.50 ppm] or ^{1}H [Trimethylsilane: ^{1}H(δ) = 0 ppm] and ^{13}C [$CDCl_3$: ^{13}C(δ) = 77.16 ppm]. Absolute values of the coupling constants were given in Hertz (Hz), regardless of their sign. Multiplicities were abbreviated as singlet (s), doublet (d), triplet (t), and multiplet (m). Data collection for X-ray crystal analysis was performed on a Rigaku/XtaLAB Synergy-S/Cu (Mo–Kα λ = 0.7107 Å) diffractometer. The X-ray measurement was performed at −160 °C or at room temperature (25 °C). The structures were solved by direct methods (SHELXT) and refined through full-matrix least-squares techniques on F^2 using SHELXL and OLEX2 crystallographic software packages. PL and those excitation spectra were measured on a JASCO model FP-8500 spectrophotometer. Absolute quantum yield was obtained using Hamamatsu C9920-02. Optical microscopy fluorescence images were obtained using SHIMADZU moticam 1080BMH with WUBEN E19 UV 365 nm. Examination of the ASE properties was performed using a fiber-coupled spectrometer (HRS-300S-NI-KKAS) equipped with a CCD detector (PIXIS-256E-KKAS), and a Nd:YAG laser ($\lambda_{3\omega}$ = 355 nm, >5 ns pulse duration, 1 kHz repetition) as an optical excitation source.

Theoretical calculations

TD-DFT calculations were performed using the Gaussian 03 suite of programs and the B3LYP/6-31G methods. The orbital diagrams were generated using the GaussView program.[36]

Conclusions

We examined the effect of fluorination on the aggregation motif and ASE performance for the widely used solid-state laser media; the **DSB** backbone. Fluorination at vinylene units promoted intermolecular CH–π interactions, resulting in a herringbone packing motif. In contrast, fluorination at the central phenylene unit led to a π-stacked aggregation motif. Crystals exhibiting herringbone packing showed larger radiative rate constant k_r values, while those with a π-stacked aggregation motif exhibited smaller k_r values. Fluorinated **DSB** derivatives with larger k_r values demonstrated ASE, whereas the compounds with smaller k_r values did not exhibit ASE. Therefore, we successfully proposed a rational molecular design strategy to achieve lasing by introducing substituents into the vinylene unit.

Author contributions

T. M. designed the research, performed experiments, and wrote the manuscript. S. H. revised the manuscript. D. F. and S. I. contributed to designing the compounds.

Conflicts of interest

There are no conflicts to declare.

Data availability

The data supporting this article have been included as part of the supplementary information (SI). Supplementary information is available. See DOI: https://doi.org/10.1039/d5ma01220a.

CCDC 2475422, 2475424, 2475425 and 2475426 contain the supplementary crystallographic data for this paper.[37a–d]

Acknowledgements

S. H. acknowledges the JST FOREST Program (no. JPMJFR211W) and a KAKENHI grant (Grant-in-Aid for Scientific Research B: no. 24K01574) of the Japan Society for the Promotion of Science (JSPS). T. M. acknowledges a KAKENHI grant (Grant-in-Aid for Young Scientific Research: no. 22K14671), and a Scientific Research Grant from ''Iketani Science and Technology Foundation'' and ''Takahashi Industrial and Economic Research Foundation''. The authors acknowledge Prof. Dr Akitaka Ito at Kochi University of Technology for measurements of PL lifetime.

References

1 Q. Zhang, W. Tao, J. Huang, R. Xia and J. Cabanillas-Gonzalez, *Adv. Photonics Res.*, 2021, **2**, 2000155.
2 J. Gierschner, S. Varghese and S. Y. Park, *Adv. Opt. Mater.*, 2016, **4**, 348–364.
3 Y. Wang, X. Han, L. Jin, Y. Meng, C. Jiang, K. Asare-Yeboah, Z. He and S. Bi, *Coatings*, 2023, **13**, 1815.
4 T. Matsuo and S. Hayashi, *J. Phys. Chem. Lett.*, 2024, **15**, 3968–3974.
5 Z. Zhuo, C. Wei, M. Ni, J. Cai, L. Bai, H. Zhang, Q. Zhao, L. Sun, J. Lin, W. Liu, X. Ding, K. Shen and W. Huang, *Dyes Pigm.*, 2022, **204**, 110425.
6 J.-J. Wu, H. Gao, R. Lai, M.-P. Zhuo, J. Feng, X.-D. Wang, Y. Wu, L.-S. Liao and L. Jiang, *Matter*, 2020, **2**, 1233–1243.
7 T. Matsuo, S. Azuma, M. Nakabayashi, F. Sasaki and S. Hayashi, *Adv. Opt. Mater.*, 2025, **13**, 2402701.
8 S. Varghese, S. K. Park, S. Casado, R. C. Fischer, R. Resel, B. Milián-Medina, R. Wannemacher, S. Y. Park and J. Gierschner, *J. Phys. Chem. Lett.*, 2013, **4**, 1597–1602.
9 M. Nakabayashi, T. Matsuo and S. Hayashi, *Chem. – Eur. J.*, 2025, **31**, e202501326.
10 H. Mochizuki, *Appl. Phys. Express*, 2019, **12**, 041007.
11 T. Matsuo, F. Sasaki and H. Yanagi, *Appl. Phys. Express*, 2022, **15**, 051002.
12 T. Kanagasekaran, H. Shimotani, K. Kasai, S. Onuki, R. D. Kavthe, R. Kumashiro and K. Tanigaki, *arXiv*, 2019, preprint, arXiv:1903.08869, DOI: 10.48550/arXiv.1903.08869.
13 K. Bando, H. Fujii, K. Mizuno, K. Narushima, A. Miyazaki, F. Sasaki, S. Hotta and H. Yanagi, *ChemNanoMat*, 2018, **4**, 936.
14 W. Takahashi, K. Maruyama, J. Li, M. Imakawa and T. Takenobu, *Jpn. J. Appl. Phys.*, 2014, **53**, 02BB02.
15 Q. Chen, B. Tang, K. Ye, H. Hu and H. Zhang, *Angew. Chem., Int. Ed.*, 2025, **64**, e202417459.
16 M. Nakabayashi, T. Matsuo and S. Hayashi, *Chem. – Eur. J.*, 2023, **29**, e2023023.

17 M. Annadhasan, A. V. Kumar, P. Giri, S. Nandy, M. K. Panda, K. V. J. Jose and R. Chandrasekar, *Angew. Chem., Int. Ed.*, 2023, **62**, e202302929.
18 M. Rohullah, V. V. Pradeep, S. Singh and R. Chandrasekar, *Nat. Commun.*, 2024, **15**, 4040.
19 L. Catalano, D. P. Karothu, S. Schramm, E. Ahmed, R. Rezgui, T. J. Barber, A. Famulari and P. Naumov, *Angew. Chem., Int. Ed.*, 2018, **57**, 17254–17258.
20 T. Matsuo, K. Ikeda and S. Hayashi, *Aggregate*, 2023, **4**, e378.
21 G. Zhao, H. Dong, Q. Liao, J. Jiang, Y. Luo, H. Fu and W. Hu, *Nat. Commun.*, 2018, **9**, 4790.
22 T. Seki, S. Kobayashi, R. Ishikawa, K. Yano, T. Matsuo and S. Hayashi, *Chem. Sci.*, 2024, **15**, 12258–12263.
23 S. Hayashi and T. Koizumi, *Angew. Chem., Int. Ed.*, 2016, **55**, 2701.
24 S. Hayashi, S. Yamamoto, D. Takeuchi, Y. Ie and K. Takagi, *Angew. Chem., Int. Ed.*, 2018, **57**, 17002.
25 T. Matsuo and S. Hayashi, *J. Mater. Chem. C*, 2025, **13**, 9527–9535.
26 K. Yano, T. Matsuo and S. Hayashi, *J. Mater. Chem. C*, 2025, **13**, 9527–9535.
27 Y. Shimomura, K. Igawa, S. Sasaki, N. Sakakibara, R. Goseki and G. Konishi, *Chem. – Eur. J.*, 2022, **28**, e202201884.
28 Z. Shi, J. Davies, S. Jang, W. Kaminsky and A. K.-Y. Jen, *Chem. Commun.*, 2012, **48**, 7880–7882.
29 J. Gierschner and S. Y. Park, *J. Mater. Chem. C*, 2013, **1**, 5818–5832.
30 D. Furusho, N. Shida, R. Hifumi, I. Tomita and S. Inagi, *J. Org. Chem.*, 2023, **88**, 14820–14825.
31 A. Y. Sosorev, V. A. Trukhanov, D. R. Maslennikov, O. V. Borshchev, R. A. Polyakov, M. S. Skorotetcky, N. M. Surin, M. S. Kazantsev, D. I. Dominskiy, V. A. Tafeenko, S. A. Ponomarenko and D. Y. Paraschuk, *ACS Appl. Mater. Interfaces*, 2020, **12**, 9507–9519.
32 I. P. Koskin, C. S. Becker, A. A. Sonina, V. A. Trukhanov, N. A. Shumilov, A. D. Kuimov, Y. S. Zhuravleva, Y. O. Kiseleva, I. K. Shundrina, P. S. Sherin, D. Y. Paraschuk and M. S. Kazantsev, *Adv. Funct. Mater.*, 2021, **31**, 2104638.
33 D. R. Maslennikov, D. I. Dominskiy, A. Y. Sosorev, V. A. Trukhanov, V. G. Konstantinov, N. I. Sorokina, O. V. Borshchev, M. S. Skorotetcky, S. A. Ponomarenko and D. Y. Paraschuk, *J. Phys. Chem. C*, 2024, **128**, 9364–9375.
34 S. Gámez-Valenzuela, M. Comi, S. R. González, M. C. R. Delgado, M. Al-Hashimi and R. P. Ortiz, *J. Mater. Chem. C*, 2023, **11**, 8027–8036.
35 A. Y. Sosorev, V. A. Trukhanov, M. S. Skorotetcky, R. A. Polyakov, V. G. Konstantinov, D. I. Dominskiy, V. A. Tafeenko, O. V. Borshchev, S. A. Ponomarenko and D. Y. Paraschuk, *J. Phys. Chem. C*, 2025, **129**, 10652–10663.
36 M. J. Frisch, G. W. Trucks, H. B. Schlegel, G. E. Scuseria, M. A. Robb, J. R. Cheeseman, J. A. Montgomery Jr., T. Vreven, K. N. Kudin, J. C. Burant, J. M. Millam, S. S. Iyengar, J. Tomasi, V. Barone, B. Mennucci, M. Cossi, G. Scalmani, N. Rega, G. A. Petersson, H. Nakatsuji, M. Hada, M. Ehara, K. Toyota, R. Fukuda, J. Hasegawa, M. Ishida, T. Nakajima, Y. Honda, O. Kitao, H. Nakai *et al. Gaussian 03, Revision C.02*, Gaussian, Inc., Wallingford, CT, 2004.
37 (*a*) CCDC 2475422: Experimental Crystal Structure Determination, 2025, DOI: **10.5517/ccdc.csd.cc2p2wb0**; (*b*) CCDC 2475424: Experimental Crystal Structure Determination, 2025, DOI: **10.5517/ccdc.csd.cc2p2wd2**; (*c*) CCDC 2475425: Experimental Crystal Structure Determination, 2025, DOI: **10.5517/ccdc.csd.cc2p2wf3**; (*d*) CCDC 2475426: Experimental Crystal Structure Determination, 2025, DOI: **10.5517/ccdc.csd.cc2p2wg4**.